Electronic Supplementary Information

EXPERIMENTAL METHODS

Materials

TiO_2 powder (Rutile, "Nano-Rutil" E3-692-011-009, Sachtleben, Germany), $Fe(NO_3)_3 \cdot 9H_2O$ (ACS reagent, $\geq$ 98 %, Riedel-de-Haën), $Cu(NO_3)_2 \cdot 3H_2O$ (purum. p.a., 98.0-103 % (RT), Sigma-Aldrich), H_2PtCl_6 (ACS, Premion 99.95 % (metal basis), Pt 37.5 %, Sigma-Aldrich), methanol (99.8 %, VWR BDH Prolabo), tert-butanol (ACS reagent, $\geq$ 99.0 %, Sigma-Aldrich), EDTA (ACS reagent, 99.0 – 101.0 %, Sigma-Aldrich), tetranitromethane (Sigma-Aldrich), and 4-chlorophenol ($\geq$ 99.0 %, Fluka) were used as received.

Synthesis of $TiO_2(R)$-Cu, $TiO_2(R)$-Fe, and reference materials

$TiO_2(R)$-Cu and $TiO_2(R)$-Fe with optimized Cu and Fe loading was prepared via an impregnation technique as described previously.[S1] A suspension of TiO_2 (rutile, 2.0 g, 25.0 mmol) and distilled water (50 mL) was sonicated for 5 min. Afterwards, the suspension was thoroughly stirred and $Cu(NO_3)_2 \cdot 3H_2O$ (8.5 mg, 0.7 mmol/L) or $Fe(NO_3)_3 \cdot 9H_2O$ (20.2 mg, 1.0 mmol/L) was added to the suspension. The suspension was stirred for further 24 h at RT and, subsequently, centrifuged at 4000 rpm for 15 min. The product was dried at 80 °C for 3 h followed by heating at for 1h at 120 °C ($TiO_2(R)$-Fe), and at 150 °C ($TiO_2(R)$-Cu) respectively.

Reference CuO_x and FeO_x were prepared by precipitation of copper and iron hydroxides from nitrate solutions, followed by filtration and drying at 150 °C. Further calcination at 450 °C for two hours yielded reference CuO and Fe_2O_3 materials.

Synthesis of $TiO_2(R)$-Pt

$TiO_2(R)$-Pt was prepared via a photodeposition technique. TiO_2 (rutile, 1.0 g) was suspended in $H_2PtCl_6 \cdot 6H_2O$ (18 mL, 1 mmol/L) and methanol (2 mL). The suspension was thoroughly stirred and exposed under a 150 W Xe-lamp (LOT Oriel) equipped with a heat-absorbing filter (KG3, Schott) for a certain time (5, 10, 15, 20, 30, and 60 min). Afterwards, the suspension was centrifuged at 4000 rpm for 10 min. The product was dried for 3 h at 80 °C. Detailed characterization was performed on samples with optimum photocatalytic performance prepared using an irradiation time of 20 min.

Photocatalytic activity tests

The photocatalytic degradation of 4-chlorophenol (4-CP) was investigated. A solution of the pollutant (4-CP, 2.5×10^{-4} mol/L, 25 mL) was added into a borosilicate glass cell with the photocatalyst (25 mg). The obtained suspension was sonicated in the dark for 5 min. Subsequently, the reaction cell was fixed under a US-800 solar simulator (150 W xenon lamp, UNNASOL GmbH, Germany) equipped with a heat-absorbing filter (HA03, Hebo) and stirred magnetically. For visible (VIS-only) light irradiation (λ > 455 nm) a corresponding cut-off filter was used (GG455, Schott). The photocatalytic degradation was investigated for 3 h. The initial degradation rates were calculated from the degradation progress within the first

30 minutes. Samples were taken at regular intervals, collected in the dark, and then filtered through a micropore filter (Sarstedt, 0.20 μm). The UV/Vis-spectra were recorded with a Cary 60 spectrometer. The amount of total carbon was measured at the Hygiene Institut Gelsenkirchen in a dilution of 1:10. Experiments with scavengers were performed using a 10 mM solution of ETDA or t-BuOH and were carried out as ascribed above.

The photocatalytic degradation in the presence of tetranitromethane was performed with the Ushio 150 W Xenon lamp in a light-condensing lamp housing (LOT-Oriel GmbH). Argon was bubbled prior and during irradiation.

Standard deviation (σ) was calculated from more than three degradation experiments. The error bars were constructed using 2σ values (confidence interval of ~95%).

The stability of the photocatalysts were tested in four three-hour cycles. Therefore the catalyst concentration of 1.0 g/L (25 mg) and the 4-CP concentration of 2.5×10^{-4} M was used. After each cycle the photocatalyst was recovered by centrifugation (4000 rpm, 5 min) and the 4-CP concentration was adjusted to the initial value.

The efficiency of hydroxyl radical generation was estimated by measuring the photocatalytic conversion of terephthalic acid (TA) to hydroxyterephthalic acid (TAOH). Photocatalysts were irradiated in TA solution (6×10^{-3} mol/L TA, 0.01 M HCl, pH set to 6.5) for 30 min. Samples were collected in 5 min intervals. In the reaction of non-fluorescent TA with hydroxyl radicals, the formation of TAOH can be monitored by emission spectra measurements. TAOH shows a broad emission band at $\lambda_{max} = 425$ nm when excited at $\lambda_{exc} = 315$ nm. Fluorescence spectra were measured using a FluoroLog-3 (Horiba JobinYvon) spectrofluorometer in a 1 cm quartz cuvette.

Photopotential transient measurements

200 mg photocatalyst were suspended in 1mL ethanol and sonicated for 15 minutes. Then the suspension was smeared onto the FTO glass by doctor blading using a scotch tape as frame and spacer. The photoelectrodes were dried at 100 °C for 15 minutes and pressed for 2 minutes at a pressure of 200 kg/cm².

The photoelectrochemical setup consisted of a Gamry 600 Reference potentiostat and a three-electrode cell using a platinum counter electrode and a Ag/AgCl (3M KCl) reference electrode. The photoelectrodes were pressed against an O-ring of the cell leaving an irradiated area of 0.5 cm². The measurements were collected in an open circuit voltage setup. The photoelectrodes were irradiated from the backside (through the FTO glass) by monochromatic light of 350 nm (Instytut Fotonowy). The measurements were done in a pH 7 phosphate buffer under oxygen atmosphere (solution was bubbled with O_2 for 30 minutes) and repeated without oxygen (solution was bubbled for 30 minutes with Ar).

EXAFS/XANES measurements

Fe and Cu K-edge XAFS spectra were collected at room temperature in a fluorescence mode at XAFCA facility, Singapore Synchrotron Light Source (SSLS).[S2] A Bruker Xfalsh 6100 detector was used to measure the fluorescence signal. In a typical experiment, the sample was prepared as a compressed 10 mm diameter pellet and loaded into a cell. The XANES samples were measured 3 times and EXAFS of each sample were measured 10 times to improve the signal to noise ratio of the data. Fourier transformation of k^3-weighted EXAFS data were performed over the range k = 2-10 Å^{-1}. Radial distances not corrected for phase shift. XAS data was analysed using a combination of PySpline1 and Microsoft Excel2 for background

subtractions, and Artemis3 for EXAFS fitting.[A. Tenderholt, B. Hedman, K. O. Hodgson. in *XAFS13* **2007,** pp. 105-107; *MicroSoft Excel* **2007** (Microsoft Excel Copyright 2007); Ravel B., Newville M. Athena, Artemis, Hephaestus: Data analysis for X-ray Absorption Spectroscopy. *J Synchrotron Radiat.* **2005**, *12*, 537; http://cars9.uchicago.edu/~ravel/software/doc/Artemis/artemis.html.]

EPR measurements

The measurements were carried out at room temperature using the Bruker Elexsys E-500 spectrometer operating in X-band (9.8 GHz) and 100 kHz magnetic field modulation equipped with super high sensitivity cavity ER 4122 SHQE. The spectra were recorded at 2 mW microwave power, time constant 81.92 ms, conversion time 163.84 ms.

Inductively coupled plasma optical emission spectrometry (ICP-OES)

For elemental analysis an ICP-OES (UNICAM 701) was used. 25 mg of each sample was mixed with 800 mg of Na_2O_2 and fused in a Zr-cup over the flame of a Bunsen-burner. The melt was diluted in H_2O and HNO_3 and then analyzed with ICP-OES.

STEM-EELS measurements

The experiments were carried out on a FEI Titan "cubed" microscope, equipped with an aberration corrector for the probe-forming lens and operated at 120kV. The EELS spectra were acquired on a Gatan Enfinium post-column spectrometer. The convergence semi-angle α was 21 mrad, the EELS collection semi-angle β and high angle annular dark field scanning transmission electron microscopy (HAADF)-STEM inner detection semi-angle were 130 mrad respectively.

XRD measurements

X-ray diffraction spectra (XRD) were recorded using a Bruker D8 Advance Diffractometer with Mo–K(α) radiation source operating at 50 kV and 40 mA. Samples were measured in glass capillary tubes (ø 0.5 mm) with steps of 0.01º and in the range of 2θ = 5–70º.

PL measurements

Solid state photoluminescence spectra were recorded on Horiba Jobin Yvon Fluorolog under the excitation light at 340 nm. The band structure is poor-resolved due to temperature of measurement (RT) and the low power of excitation source.

THEORETICAL CALCULATIONS

All calculations were performed with the Density Functional Theory, using the VASP code.[S3] The plane wave cutoff is 420 eV, with the Projector Augmented Wave method used to treat the core electrons.[S4] The rutile phase of TiO_2 was modelled using the *GGA+U* approach to provide an accurate treatment of localized electron states.[S5] Specifically, we use a U value of 4.2 eV placed on the *d*-electrons of Ti.[S6] For the primitive unit cell, a Monkhorst-Pack *k*-point mesh of (5 × 5 × 5) *k*-points was used. The lattice parameters of the unit cell of rutile TiO_2 were obtained by generating energy-volume data from a series of constant volume cell shape

optimization calculations, and fitting this data to the Birch-Murnaghan equation of state. Lattice parameters were calculated to be $a = b = 4.584$ Å (an underestimate of 0.7% with respect to experiment) and $c = 2.972$ Å (an overestimate of 0.6% with respect to experiment).[S7] We determined the effects of metal cation sensitization on the (110) surface of rutile, as it is the most commonly observed surface facet.[S8] A supercell composed of (3×6×1) surface unit cells with a depth of 6 atomic layers was used to model this surface, with lattice parameters 19.86 Å × 18.19 Å × 25.00 Å (this includes a 15.95 Å vacuum spacing to separate periodic images along the z-axis). This is a surface density of 0.277 atoms/nm^2, of similar magnitude to experiment. The supercell model contains in total 324 atoms. For the supercell, sampling of the Γ-point was sufficient to obtain well-converged energies and forces, and the dipole correction (applied perpendicular to the surface) was used to treat surface dipole effects. We also modelled the effects of Cu(II) and Fe(III) metal ions on the (110) surface of TiO_2. Unlike for bulk systems the presence of a strong inhomegenity in the dielectric environment at surfaces means that for charged defects the correction schemes for the long-range Coulombic interactions are not valid.[S9] Therefore, in order to model metal cations on the surface we have used representative clusters that contain transition metal cations. For TiO_2(R)-Fe we modelled the adsorption of a single $Fe(OH)_3$ cluster, for the related system TiO_2(R)-Fe(V_{Ti}) we modelled the adsorption of a single FeOH cluster, while for TiO_2(R)-Cu we modelled the adsorption of a single CuO cluster. For Fe, we used a value of $U = 5.0$ eV and $J = 1.0$ eV placed on the d-electrons of Fe,[S10] whereas for Cu we used a value of $U = 9.79$ eV and $J = 2.5$ eV, placed on the d-electrons of Cu.[S11] All atoms were fully relaxed until the change in force upon ionic displacement was less than 0.01 eV/Å, with the convergence criteria for the electronic energy set to 10^{-5} eV. All calculations involving metal cations were spin-polarised.

X-RAY ABSORPTION SPECTROSCOPY DATA

EXAFS Fits of Copper EXAFS

To compare the EXAFS of the TiO_2(R)-Cu materials prepared at 150 °C and 450 °C, 3 parameter single scatting fit to the main peaks of the XAS was performed. While there are clearly more contributions than this, the idea was to limit the parameters to evaluate any structural differences between the two materials. The data were fit using the rutile structure where a copper atom replaced a titania in the structure. The S02 and E0 were kept consistent between fits to facilitate comparison. (The final numbers were chosen based on an average of free floated fits).

Both sets of XAS are well described by a copper atom doped into rutile. However, there are notable differences between the active (150 °C) and inactive (450 °C) forms. When the fits are kept the same, there is a substantial increase in the Debye Waller Factor for the Cu-Ti

distance at ~2.9Å. This is consistent with the material going from the surface into the bulk of the phase.

3 parameter fit to :TiO$_2$(R)-Cu-450 °C

Name	N	S02	σ^2	E0	ΔR	R (Rutile)	R (Fit)
Cu-O	6	0.591	0.00846	-4.417	0.0276	1.9	2.0
Cu-Ti	2	0.591	0.00364	-4.417	-0.087	2.9	2.8
Cu-Ti	8	0.591	0.00805	-4.417	-0.0219	3.6	3.6

3 parameter fit to TiO$_2$(R)-Cu-150 °C

Name	N	S02	σ^2	E0	ΔR	R (Rutile)	R (Fit)
Cu-O	6	0.591	0.00749	-4.417	0.0206	1.947	1.967
Cu-Ti	2	0.591	0.00784	-4.417	-0.0987	2.957	2.859
Cu-Ti	8	0.591	0.00856	-4.417	-0.0418	3.568	3.526

3 parameter fit to CuO

Name	N	S02	σ^2	E0	ΔR	R (Tenorite)	R (Fit)
Cu-O	4	0.661	0.0032	-1.64	-0.005	1.96	1.95
Cu-Cu	10.0	0.661	0.021	-1.64	0.1	2.9	3.0
Cu-Cu	2.0	0.661	0.007	-1.64	0.1	3.8	3.9
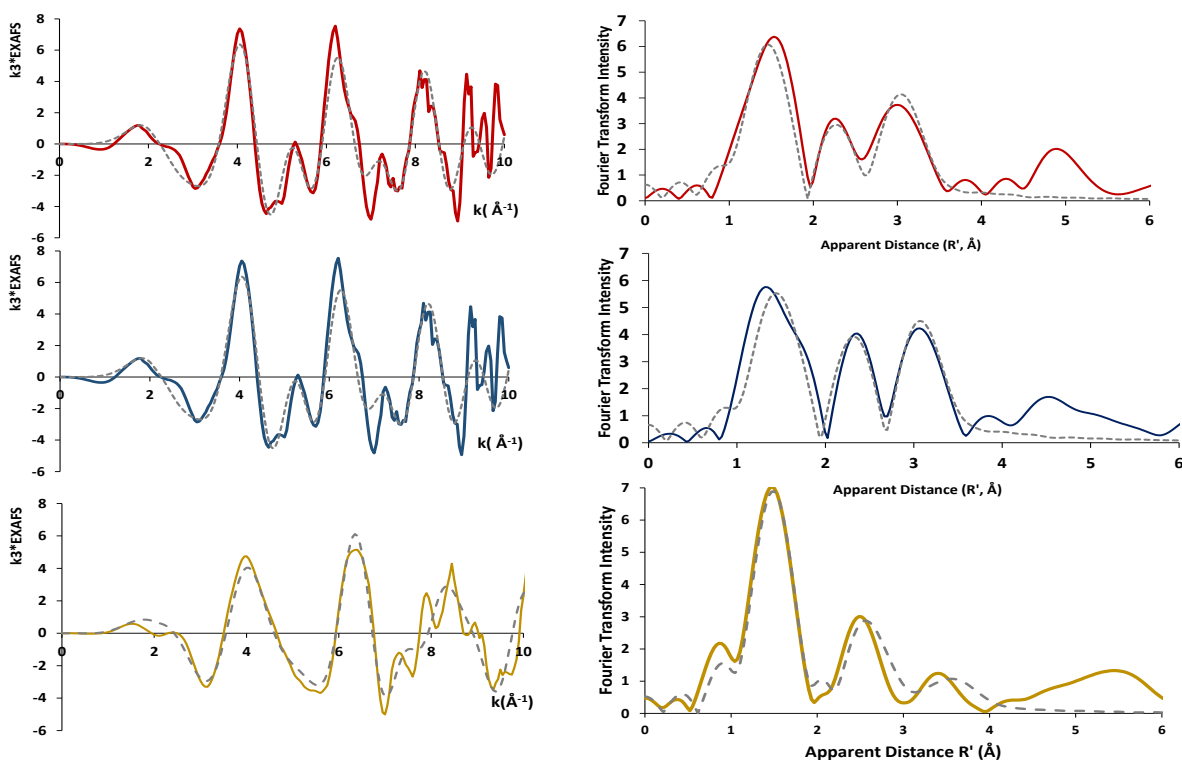
red---: TiO₂(R)-Cu 150°C active
blue---: TiO₂(R)-Cu 150°C active
yellow---: CuOx reference (150°C)

Fig. S1. EXAFS simulations based on a 3 parameter fits. The first two fits include 6x Cu-O (unsplit) @ 1.95Å, 2x Cu-Ti @2.9Å and 8x Cu-Ti @ 3.5 Å. The parameters in the fit were minimized to facilitate comparison. The final fit is to CuO based on the tenorite structure. The fits are intended as a comparison only.

3 parameter fit to TiO$_2$(R)-Fe (120 °C) Note: the XAS data quality of the Fe containing samples was not as good as for the Cu containing samples

Name	N	S02	σ^2	E0	ΔR	R (Rutile)	R (Fit)
Fe-O	6	0.434	0.0015	-1.720	0.043	1.94	1.99
Fe-Ti	4	0.434	0.0086	-1.720	0.093	2.96	3.05
Fe-Ti	8	0.434	0.0161	-1.720	-0.016	3.56	3.55
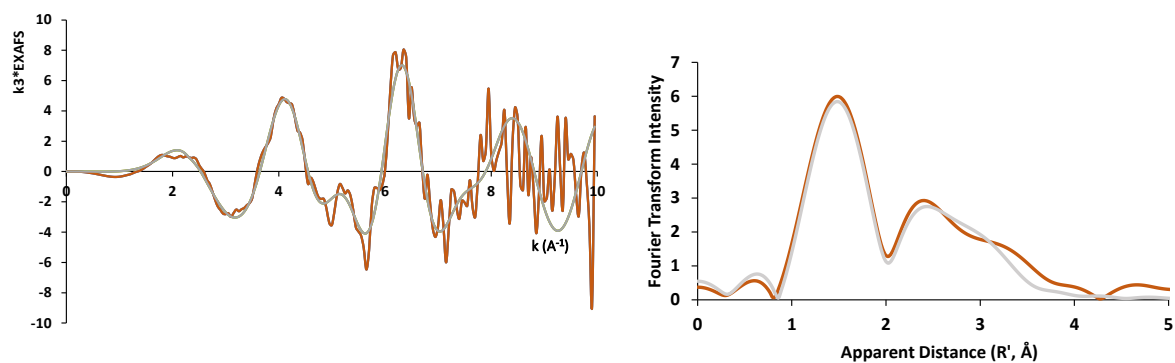
Fig. S2. EXAFS simulations based on a 3 parameter fits to the active TiO$_2$(R)-Fe material.
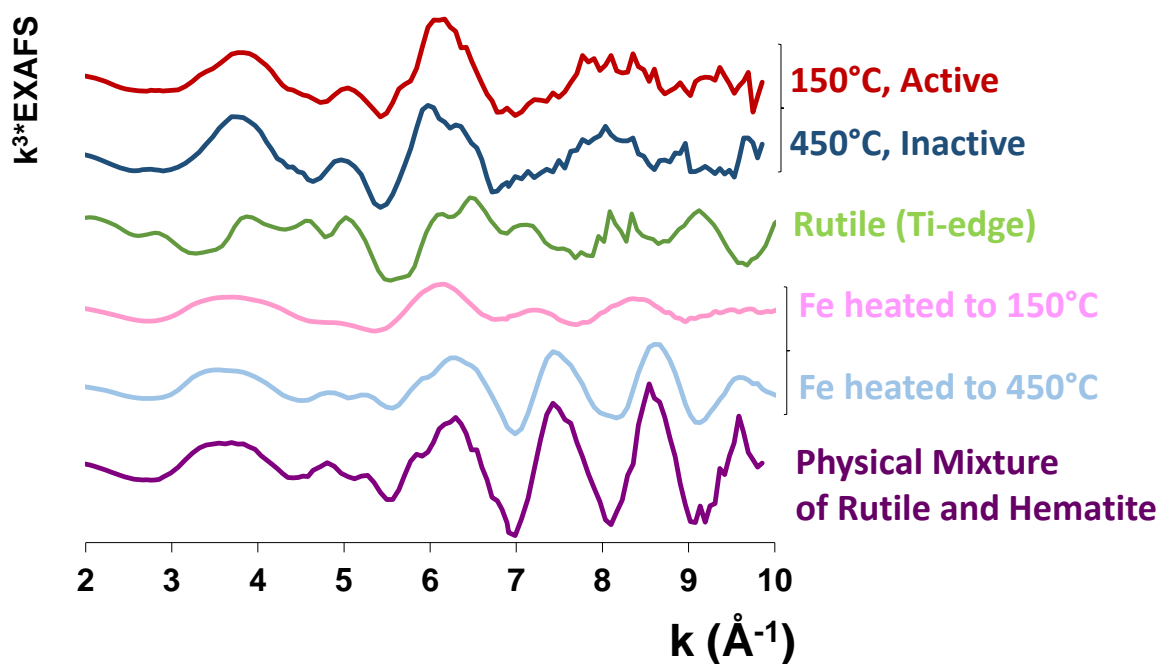
Fig. S3. EXAFS data taken at the Fe edge. Six samples are compared: the active and inactive $TiO_2(R)$-Fe materials, rutile TiO_2 taken at the Ti-edge, the reference FeO_x and Fe_2O_3 samples prepared at two different temperatures, and a physical mixture of rutile and hematite Fe_2O_3. The EXAFS are consistent with the Fe(III) on the rutile surface as being distinct phase from hematite and a physical mixture of TiO_2 and Fe_2O_3.
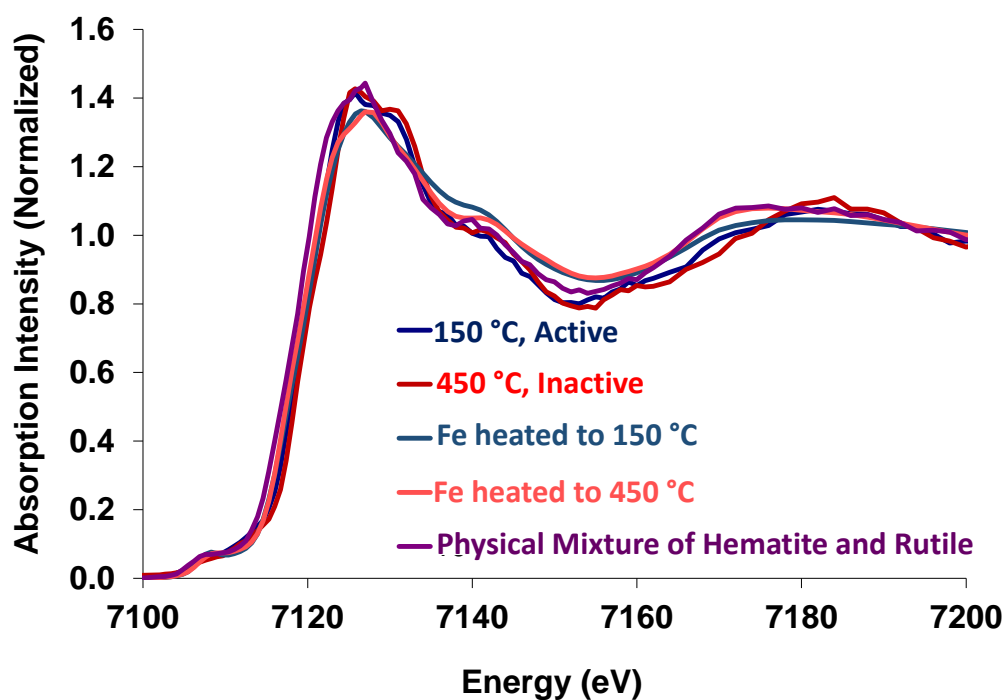
Fig. S4. XANES on the Fe samples. The data are consistent with Fe in a high spin Fe(III) configuration.
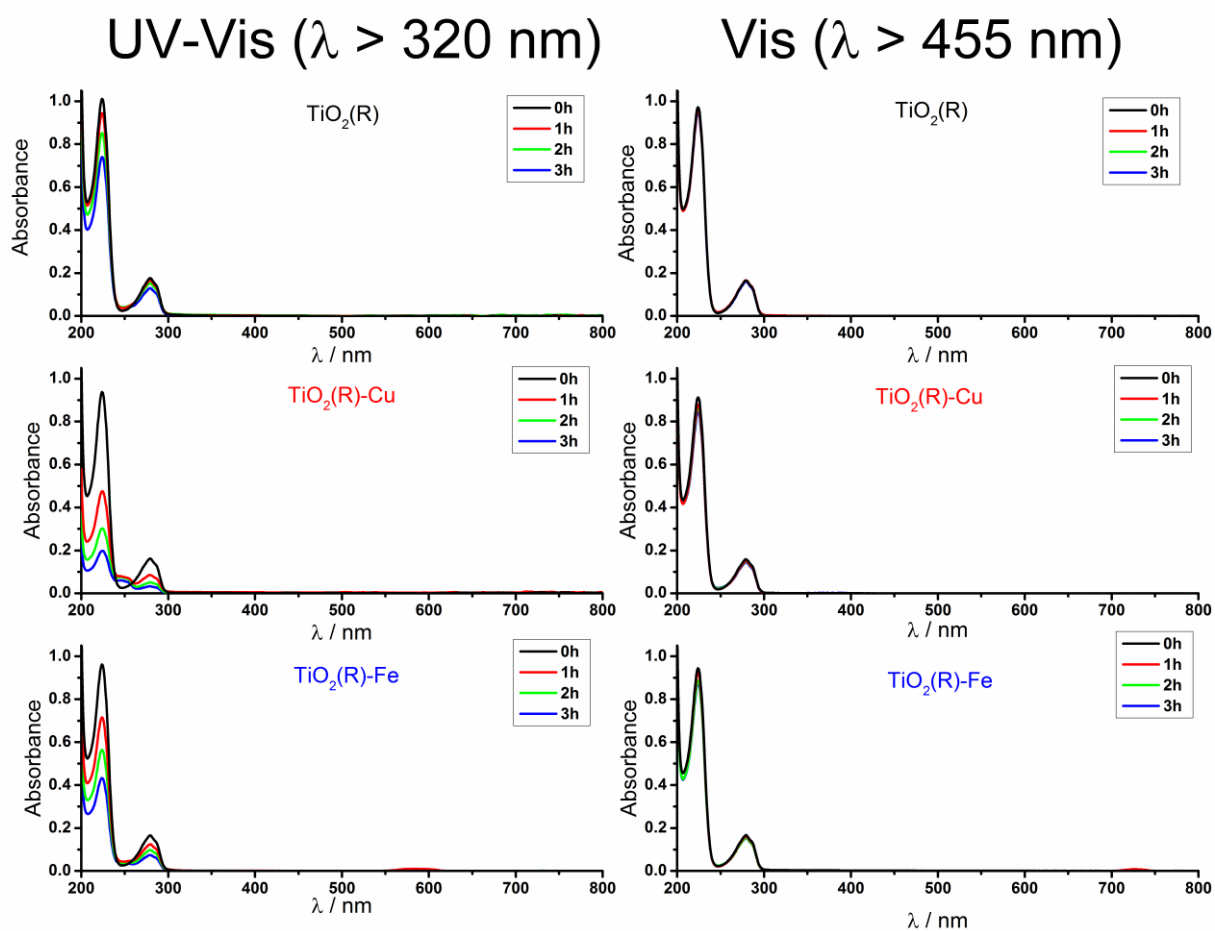
Fig. S5. UV-Vis spectra recorded in the course of 4-CP degradation experiments.
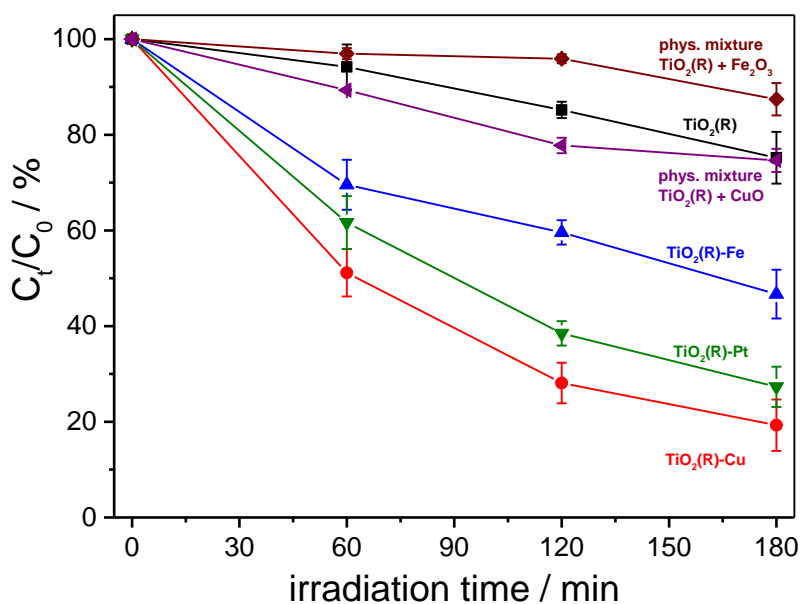
Fig. S6. Comparison of 4-CP degradation with physical mixtures of TiO_2 with CuO and Fe_2O_3.
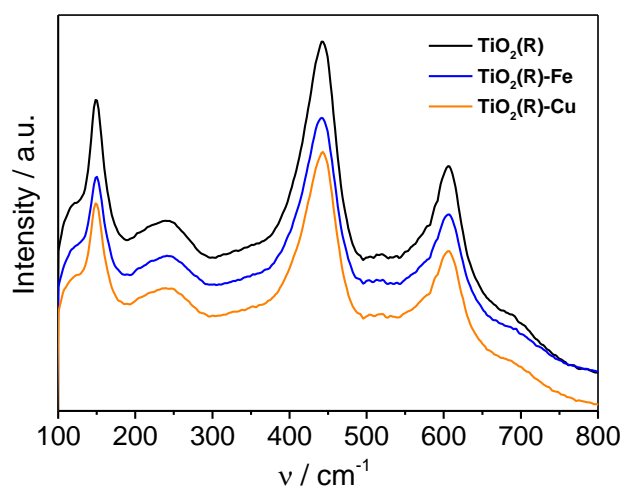
Fig. S7 Raman spectra of $TiO_2(R)$, $TiO_2(R)$-Cu and $TiO_2(R)$-Fe. Raman spectra could theoretically provide information on a local structure changes that are induced by introducing Cu(II) or Fe(III) sites. However, due to low concentration of the species, only the characteristic atomic vibrations corresponding to the rutile phase were recorded: 150 (B_{1g} mode), 242, 442 (E_g) and 606 (A_{1g}) cm^{-1}. Literature values of Raman spectra for rutile TiO_2 are 144, 235, 320-360, 448, 612 and 827 cm^{-1}.[S12,13]
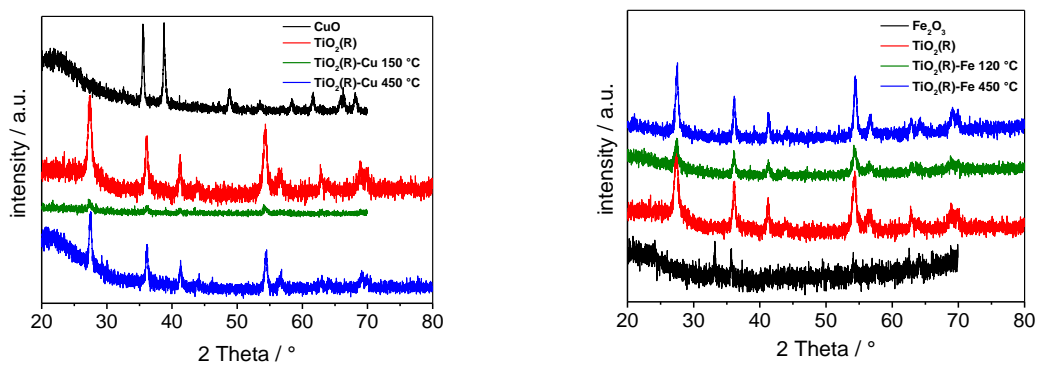
Fig. S8. XRD patterns of $TiO_2(R)$-Cu (150 °C), $TiO_2(R)$-Fe (120 °C) and reference materials.
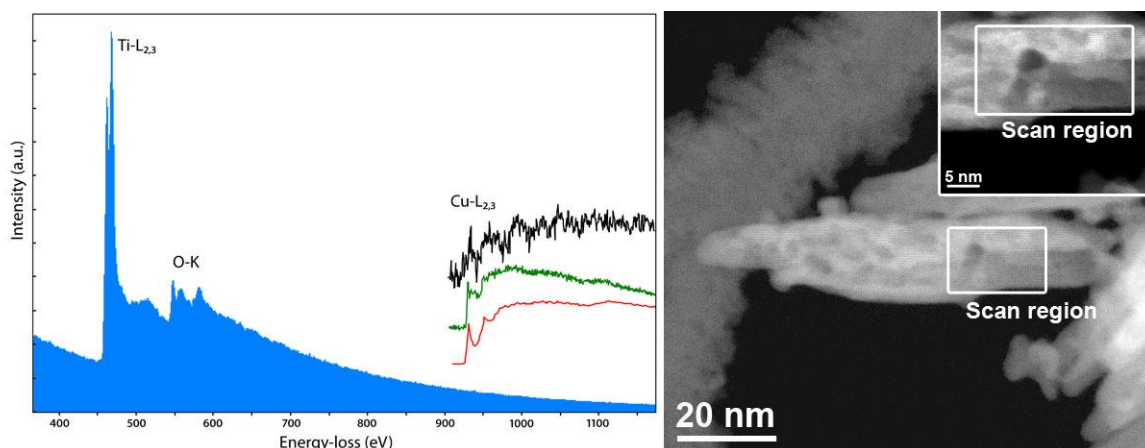
Fig. S9: EELS spectrum of $TiO_2(R)$-Cu (left) acquired from the scan region indicated by the white rectangle in the low and high magnification HAADF-STEM images on the right. Strong $Ti-L_{2,3}$ and O-K edges, corresponding to TiO_2, are apparent. A very faint $Cu-L_{2,3}$ signal (black spectrum = background subtracted $Cu-L_{2,3}$ edge) is also measured. For comparison, reference spectra for CuO (red spectrum) and Cu (green spectrum) are shown. As the signal is very low, the determination of oxidation state is difficult. Note that no Fe signal could be detected for $TiO_2(R)$-Fe.
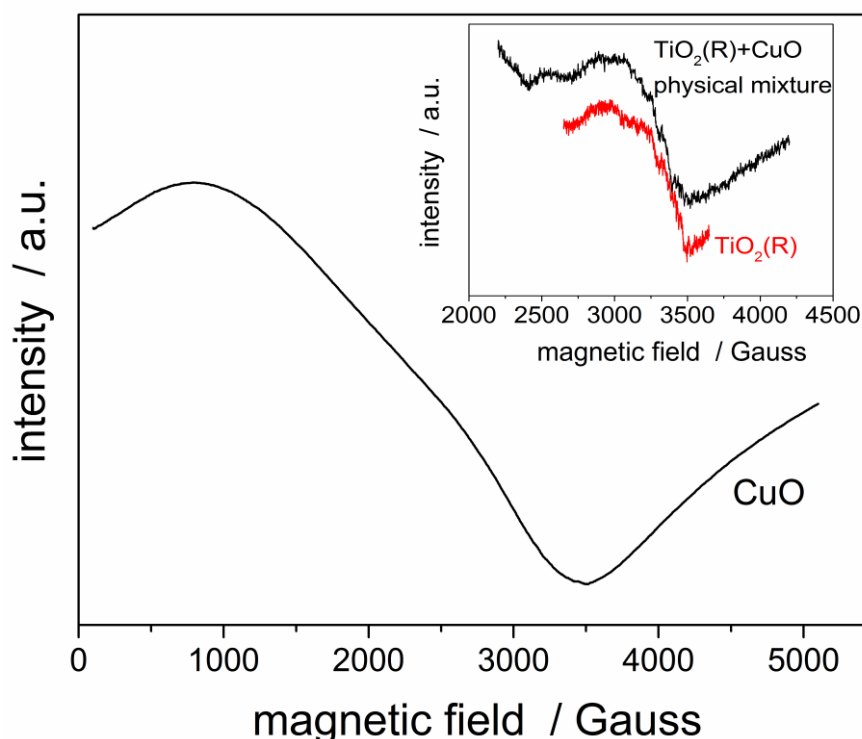
Fig. S10. EPR spectra of reference CuO powder. The inset shows EPR spectra of pristine rutile $TiO_2(R)$ and a physical mixture of TiO2(R) with CuO (0.1 wt. %).
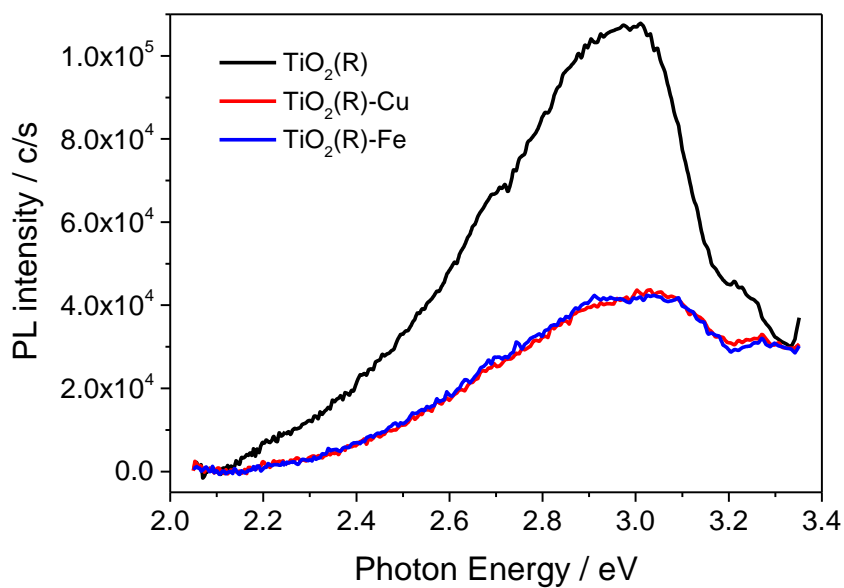
Fig. S11. Photoluminescence spectra of $TiO_2(R)$, $TiO_2(R)$-Cu and $TiO_2(R)$-Fe.
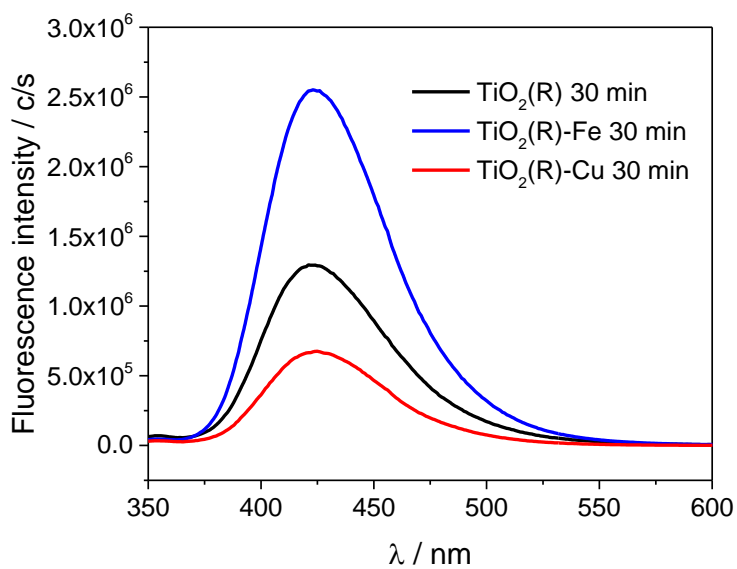
Fig. S12. Fluorescence spectra of hydroxyterephthalic acid formed upon irradiation for 30 min of the materials suspended in a solution of terephthalic acid (pH 6.5).
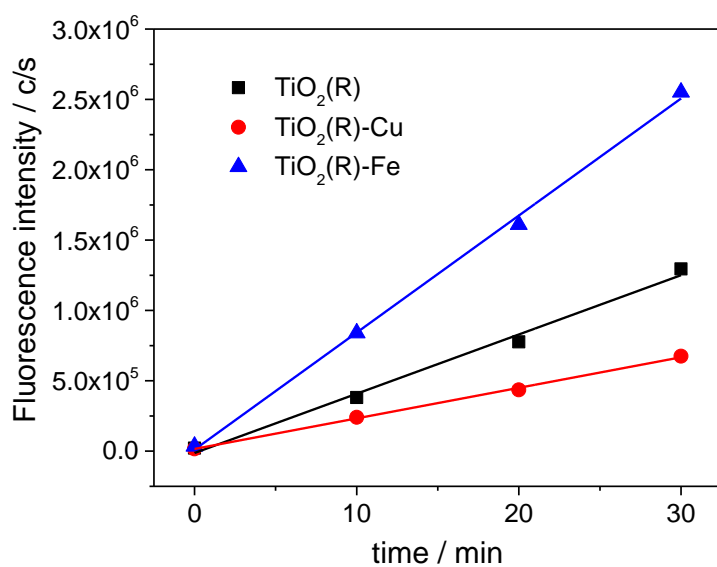
Fig. S13. The time dependence of the hydroxyterephthalic acid fluorescence intensity at λ_{max} = 424 nm.
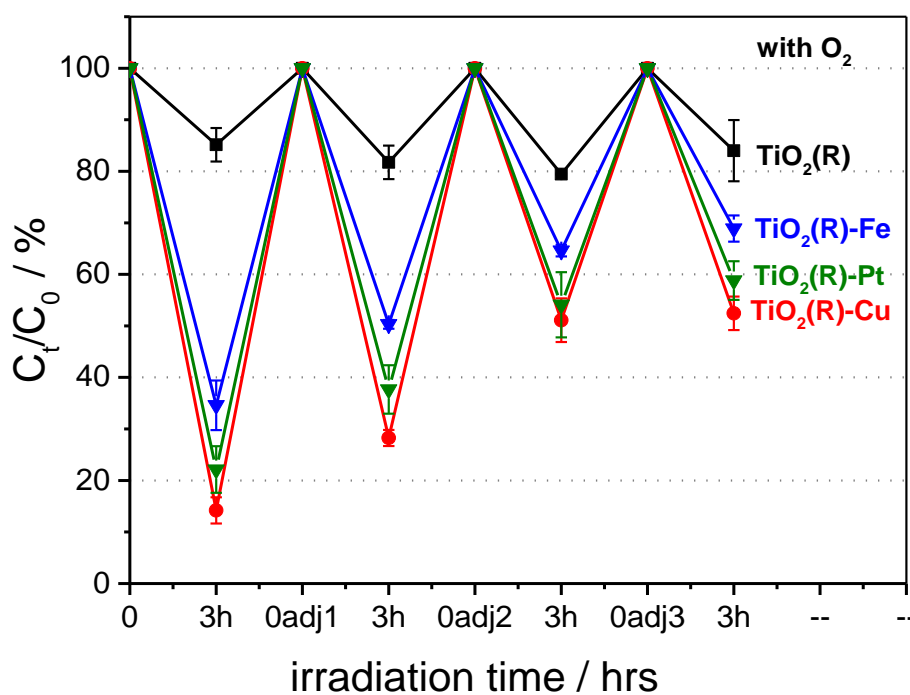
Fig. S14. The operational stability measurements under UV-Vis light ($\lambda > 320$ nm). Four successive photodegradation experiments (4-CP) were performed.

References

S1.   S. Neubert, P. Pulisova, C. Wiktor, P. Weide, B. Mei, D. A. Guschin, R. A. Fischer, M. Muhler and R. Beranek, *Catal. Today*, 2014, **230**, 97-103.

S2.   Y. Du, Y. Zhu, S. Xi, P. Yang, H. O. Moser, M. B. H. Breese and A. Borgna, *J. Synchrotron Rad.*, 2015, **22**, 839-843.

S3.   G. Kresse and J. Furthmüller, *Comp. Mater. Sci.*, 1996, **6**, 15-50.

S4.   P. E. Blöchl, *Phys. Rev. B*, 1994, **50**, 17953-17979.

S5.   S. L. Dudarev, G. A. Botton, S. Y. Savrasov, C. J. Humphreys and A. P. Sutton, *Phys. Rev. B*, 1998, **57**, 1505-1509.

S6.   B. J. Morgan and G. W. Watson, *Surf. Sci.*, 2007, **601**, 5034-5041.

S7.   J. K. Burdett, T. Hughbanks, G. J. Miller, J. W. Richardson and J. V. Smith, *J. Am. Chem. Soc.*, 1987, **109**, 3639-3646.

S8.   H. Perron, C. Domain, J. Roques, R. Drot, E. Simoni and H. Catalette, *Theor. Chem. Acc.*, 2007, **117**, 565-574.

S9.   H.-P. Komsa and A. Pasquarello, *Phys. Rev. Lett.*, 2013, **110**, 095505.

S10.   A. Rohrbach, J. Hafner and G. Kresse, *Phys. Rev. B*, 2004, **70**, 125426.

S11.   B. Himmetoglu, R. M. Wentzcovitch and M. Cococcioni, *Phys. Rev. B*, 2011, **84**, 115108.

S12.   U. Balachandran and N. G. Eror, *J. Solid State Chem.*, 1982, **42**, 276-282.

S13.   O. Frank, M. Zukalova, B. Laskova, J. Kurti, J. Koltai and L. Kavan, *Phys. Chem. Chem. Phys.*, 2012, **14**, 14567-14572.